Liquid Crystals
Publication details, including instructions for authors and subscription information:
http://www.tandfonline.com/loi/tlct20

Experimental relationship between surface and bulk rotational viscosities in nematic liquid crystals

P. Oswald [a] , G. Poy [a] , F. Vittoz [a] & V. Popa-Nita [a b]
[a] Physics Laboratory, Ecole Normale Supérieure de Lyon , University of Lyon , 69364 , Lyon , Cedex 07 , France
[b] Faculty of Physics , University of Bucharest , Bucharest , 077125 , Romania
Published online: 10 Apr 2013.

To cite this article: P. Oswald , G. Poy , F. Vittoz & V. Popa-Nita (2013): Experimental relationship between surface and bulk rotational viscosities in nematic liquid crystals, Liquid Crystals, 40:6, 734-744

To link to this article: http://dx.doi.org/10.1080/02678292.2013.783936

Liquid Crystals, 2013
Vol. 40, No. 6, 734–744, http://dx.doi.org/10.1080/02678292.2013.783936

Taylor & Francis
Taylor & Francis Group

Experimental relationship between surface and bulk rotational viscosities in nematic liquid crystals

P. Oswald[a]*, G. Poy[a], F. Vittoz[a] and V. Popa-Nita[a,b]

[a]*Physics Laboratory, Ecole Normale Supérieure de Lyon, University of Lyon, 69364 Lyon, Cedex 07, France;* [b]*Faculty of Physics, University of Bucharest, Bucharest 077125, Romania*

(*Received 20 February 2013; final version received 6 March 2013*)

Systematic measurements of the surface viscosity γ_S of several nematic liquid crystals in contact with a polymercaptan layer show that the latter scales like the bulk rotational viscosity γ_1. This result is interpreted in the framework of a 'delocalized model' for the surface viscosity.

Keywords: nematic liquid crystals; sliding anchoring; rotational surface viscosity; rotational bulk viscosity; polymercaptan layer

1. Introduction

An important question in the physics of nematic liquid crystals is the way in which the molecules 'anchor' on the surfaces limiting the samples. This property depends on the nature of the surfaces and their chemical and (or) mechanical treatments.[1–3] The anchoring is considered strong when it permanently fixes molecular orientation ('geometric' anchoring condition) and weak otherwise. In the latter case, the angle between the director and the preferred anchoring direction can change. As a result, the director experiences two torques at the surface, namely an anchoring torque $\vec{\Gamma}_a$ proportional to the anchoring energy W_a and a viscous torque of expression

$$\vec{\Gamma}_S = \gamma_S \vec{n} \times \frac{\partial \vec{n}}{\partial t}, \tag{1}$$

where γ_S is a surface viscosity introduced for the first time by de Gennes in 1974.[4] In this phenomenological approach, γ_S describes an additional dissipation due to the interaction between the surface treatment and the liquid crystal. So far, very few measurements of γ_S have been reported in spite of the numerous theoretical articles dealing with its role during the director reorientation in the presence of an external time dependent field.[5–11] One can cite an estimate of γ_S for the homeotropic anchoring by Petrov et al.[12] and another by Čopič et al.[13,14] for the planar unidirectional anchoring. Recently, we have measured γ_S in the case of sliding planar anchoring, when the molecules orient parallel to the surface but do not memorise any particular direction. In this limit, the anchoring energy vanishes and the only surface torque is the viscous torque given in Equation (1). In practice, our sliding anchoring was obtained by spin-coating a thin polymercaptan layer on the surfaces.[15] This liquid polymer is used as a hardener for the epoxy resins. This surface treatment was used to study the Lehmann effect in a compensated cholesteric mixture composed of 50% by weight of octyloxycyanobiphenyl (8OCB) and 50% of cholesteryl choride (CC).[16–19] The surface viscosity γ_S of this mixture was estimated at the compensation temperature by using a very special technique taking advantage of the rapid variation of the cholesteric pitch during temperature ramps.[15] Because this technique was not applicable to nematic or usual cholesteric liquid crystals, nor very precise, we recently developed a new method using a rotating magnetic field and which works for any nematic liquid crystals at any temperatures.[20] We showed that the concept of surface viscosity was pertinent experimentally and measured the surface viscosity for the liquid crystal 5CB (4-pentyl-4′-cyanobiphenyl) in contact with a polymercaptan layer.

The goal of the paper, which may be considered as a sequel to our previous letter,[20] is to determine whether there exists a relationship between the bulk and surface viscosities. To tackle this question, we systematically measured the two viscosities with several materials (all from Frinton Laboratories), namely MBBA (p-methyloxybenzilidene- *p*-n-butylaniline), n-cyanobiphenyls (nCB) with $n = 5$–9, and the compensated cholesteric mixture mentioned above. The two viscosities were measured by an optical method by submitting samples treated for homeotropic or planar sliding anchoring to a rotating magnetic field. The theoretical background of the measurements and the way they were conducted are recalled in Sections 2 and 3, respectively. Experimental results are given in

*Corresponding author. Email: patrick.oswald@ens-lyon.fr

Section 4 and discussed in the framework of the 'delocalised' model of Barbero et al.[7] in Section 5. Finally, conclusions are drawn and perspectives for future works are given in Section 6.

2. Theoretical background

We consider a nematic slab between two parallel glass plates treated for homeotropic or planar sliding anchoring. The liquid crystal is submitted to a magnetic field $\vec{B}$ parallel to the glass plates (plane (x, y)) which rotates with the angular velocity ω. Under the action of $\vec{B}$, the director field rotates and deforms because of the anchoring and the friction of the molecules on the surfaces. Two cases must be considered depending on the boundary conditions.

2.1 *Strong homeotropic anchoring*

In this case, the director remains perpendicular to the surfaces – so that there is no friction on the surfaces – and aligns parallel to the magnetic field at large distance from the surfaces. 'Large' here means larger than the magnetic coherence length. Let ϕ be the angle between the x-axis and the director projection $\vec{n}_{\|}$ onto the horizontal plane (x, y) (Figure 1). The resolution of the bulk torque equation by Brochard et al.[21] showed that ϕ is independent of z and given by

$$\phi = \omega t - \alpha_e \quad \text{with} \quad \alpha_e = \frac{1}{2}\arcsin\left(\frac{2\,\mu_0\gamma_1\omega}{\chi_a B^2}\right), \quad (2)$$

where μ_0 is the vacuum permittivity and χ_a is the magnetic anisotropy of the nematic phase. This solution is possible only when $\omega < \omega_c$ with $\omega_c = \frac{\chi_a B^2}{2\mu_0\gamma_1}$. This defines the synchronous regime in which the retardation angle α_e varies from 0 to $\pi/4$. It must be noted that this solution neglects the backflow effects which turn out to be negligible in our experiments at small angular velocities, as we shall see later.

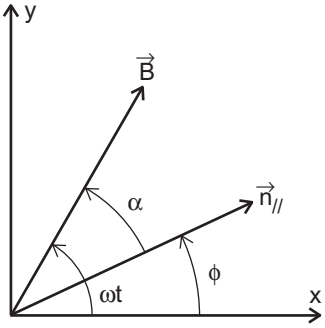

Figure 1. Definition of angles ϕ and α. The latter is the retardation angle between projection of the director onto the horizontal plane and the magnetic field.

This calculation shows that measuring the slope of the curve $\alpha_e(\omega)$ for a given value of the magnetic field allows one to deduce γ_1 on condition to know χ_a.

2.2 *Sliding planar anchoring*

In this case, the director remains everywhere parallel to the glass plates, but angle ϕ now depends on z because of the friction of the director on the surfaces. Let d be the sample thickness and K_2 be the twist Frank constant. The resolution of the bulk torque equation

$$K_2\frac{\partial^2\phi}{\partial z^2} + \frac{\chi_a}{\mu_0}B^2\sin\alpha\cos\alpha - \gamma_1\frac{\partial\phi}{\partial t} = 0, \quad (3)$$

together with the boundary conditions

$$K_2\frac{\partial\phi}{\partial z} = \gamma_S\frac{\partial\phi}{\partial t} \quad \text{at} \quad z = 0, \quad (4)$$

$$K_2\frac{\partial\phi}{\partial z} = -\gamma_S\frac{\partial\phi}{\partial t} \quad \text{at} \quad z = d, \quad (5)$$

yields in the limit $\omega \ll \omega_c$[20]:

$$\phi = \omega t - \alpha_e - \delta(z) \quad \text{with} \quad \delta(z) = \frac{\gamma_S\omega}{K_2}\frac{\cosh\left(\frac{d-2z}{2L}\right)}{\sinh\left(\frac{d}{2L}\right)}L. \quad (6)$$

Here, $L = \xi/\sqrt{\cos(2\alpha_e)}$, where $\xi = \sqrt{\frac{K_2\,\mu_0}{\chi_a}}\frac{1}{B}$ is the magnetic coherence length. This equation shows that the director field is twisted over a distance $L \approx \xi$ in the vicinity of the two surfaces. Note that *there is no backflow* in principle in this geometry as only twist deformation appears.[1] From Equations (2) and (6), we calculate the retardation angle at the surfaces when $\omega \ll \omega_c$:

$$\alpha_S = \alpha_e + \delta(0, d) = \frac{\mu_0}{\chi_a}\left[\frac{\gamma_1}{B^2} + \frac{\gamma_S}{B}\frac{\sqrt{\chi_a/(K_2\,\mu_0)}}{\tanh(d/(2\xi))}\right]\omega. \quad (7)$$

This equation shows that measuring the slope of the curve $\alpha_S(\omega)$ in the limit $\omega \to 0$ for two different values of B is sufficient to deduce γ_1 and γ_S on condition that constants K_2 and χ_a are known.

3. Principle of the measurements

The experimental setup was already described in detail in Ref.[20] (Figure 2). It was realised by one of us (F.V.). Briefly, it consists of an oven regulated to within ± 0.01°C which contains the sample and which can

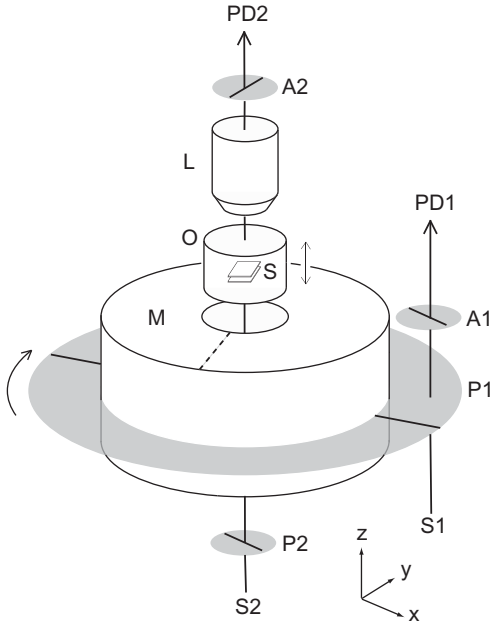

Figure 2. Schematic representation of our experimental setup. M is the rotating permanent magnet (Halbach ring of height 50 mm with a bore of 26 mm in diameter), O the oven and S the sample (of surface area $\sim 1\,\mathrm{cm}^2$). L is a microscope objective with a long working distance. PD1 and PD2 are two photodiodes. S1 is a red LED source and S2 is a white light source. P1 is a rotating polarizer attached to the magnet, P2 a fixed polariser and A1 and A2 are two fixed analysers. The dashed line drawn on the upper side of the magnet indicates the direction of the magnetic field along the revolution axis of the magnet.

move along the revolution axis of a rotating permanent magnet. In this way, the sample is submitted to a rotating magnetic field, the magnitude of which is known precisely from the position of the oven. The angle α_S between the magnetic field and the director orientation at the surfaces is deduced from the measurement of the phase shift between two signals given by two photodiodes. The first photodiode PD1 gives a signal I_1 of frequency 2ω, the phase of which Φ_1 gives the orientation of the magnetic field. The second one PD2 gives a signal I_2 of frequency 4ω, the phase of which Φ_2 gives the orientation of the director in the bulk in homeotropic anchoring and at the surfaces in planar sliding anchoring. Measuring Φ_1 and Φ_2 thus yields directly α_e in homeotropic anchoring and α_S in sliding planar anchoring by using the same formula

$$\alpha_e \quad \text{or} \quad \alpha_S = \pm\left[\frac{1}{2}\left(\Phi_1 - \frac{\Phi_2}{2}\right) + \frac{\pi}{8}\right], \qquad (8)$$

with the sign + when $\omega > 0$ and the sign − when $\omega < 0$.

In practice, I_1 and I_2 are recorded during five revolutions of the magnet and are then fitted with a sin function to obtain Φ_1 and Φ_2. Each retardation curve $\alpha_e(\omega)$ or $\alpha_S(\omega)$ is measured by varying ω from -0.6 to 0.6 rd/s by steps of 0.15 rd/s at $B = 1$ T and from -0.15 to 0.15 rd/s by steps of 0.05 rd/s at $B = 0.2$ T. All measurements and data treatments are automated with Labview and Igor Pro software. More precisely, Labview is used to control both the stepping motor driving the magnet and the data acquisition board allowing I_1 and I_2 measurements. Igor Pro is used to save and fit automatically with a sin function the intensity curves and then plot and fit with a line the curves $\alpha_e(\omega)$ or $\alpha_S(\omega)$ from which the viscosities are calculated.

We used two different methods to measure viscosities γ_1 and γ_S. Both have advantages and disadvantages which we now describe.

The first method (method 1 in the following), which was used in our previous work,[15] consists of measuring γ_1 and γ_S in the same sample treated for planar sliding anchoring. This requires to measure $\alpha_S(\omega)$ at large and small magnetic field, for instance, at $B = 1$ T and $B = 0.2$ T. This method has the advantage that the two viscosities are measured in the same sample, but it suffers from two major limitations. The first one is that each viscosity measurement at a given temperature takes about 3 hours. The reason for this is that measuring the curve $\alpha_S(\omega)$ takes about half an hour at $B = 1$ T but more than 2 hours at $B = 0.2$ T because the rotation velocity must be decreased by a factor of 5 in order that α_S remains small (typically less than 0.2 rd, see Ref.[20]). This excessive measurement time can become a problem if the polymercaptan layer degrades and pollutes the nematic sample, which was clearly the case with MBBA and the compensated mixture. Another severe limitation comes from the fact that the measurements at small magnetic field are only possible if the polymercaptan layer is 'perfect', without visible defects over a very large surface area around the central measurement zone. The reason for this is that any defect of the layer due, for instance, to a dust particle or a partial dewetting, becomes the source at small magnetic field of inversion walls (or π walls) which rapidly invade the sample (Figure 3). These walls strongly disturb the intensity measurements which must be immediately stopped.

The second method (method 2 in the following) consists of measuring α_e with a sample treated for homeotropic anchoring and α_S with a sample treated for planar sliding anchoring. In both cases, the measurements can be performed at $B = 1$ T which is the maximal value of the magnetic field in the center of the magnet bore. This new procedure has the double advantage of allowing rapid measurements while avoiding the nucleation of inversion walls. The disadvantage is that measurements are performed on two

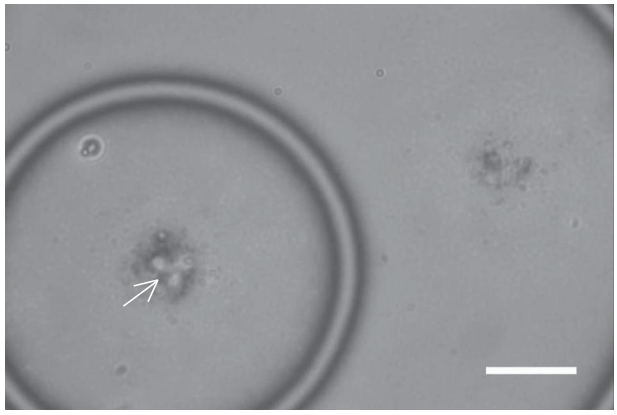

Figure 3. At the place indicated by the arrow, the polymercpatan has partly dewetted and the director cannot rotate freely. A direct consequence is the nucleation at regular intervals of time of circular π-walls centered on this zone. The smaller the magnetic field and the larger the angular velocity, the easier the nucleation is. The white bar is 100 μm long.

different samples, which can be a problem in the presence of contamination of the liquid crystal by the polymercaptan.

4. Experimental results

In practice, the sliding anchoring was obtained by depositing a thin polymercaptan layer on the glass plates according to the method described in Ref.[15]. The same polymercaptan sample was used to prepare all the samples studied in this paper. This precaution was important for reproducibility and to compare between them the surface viscosities obtained with the different liquid crystals. The homeotropic anchoring was obtained by spin-coating a thin layer of the polyimide 0626 from Nissan diluted to 5% in solvent 26 from Nissan. This layer was dried for 1 minute at 80°C and then polymerised at 160°C for 1 hour. The sample thickness was fixed to 30 μm in all experiments. Finally, we used values of the literature for χ_a and K_2 to calculate the viscosities, when they were available. More precisely, we used in the case of the cynaobiphenyls χ_a values given by Bradshaw et al.[22] (except for 8CB for which we performed new measurements, see Appendix 1) and for K_2 the data of Madhusudana and Pratibha [23] (except for 9CB for which we measured this constant, see Appendix 2). In the case of MBBA, we used the values of χ_a given by Leenhouts et al.[24] and values of K_2 given by Leenhouts and Dekker.[25] For the compensated mixture, we measured χ_a at the compensation temperature (see Appendix 1) and we used the value of K_2 we previously measured with Dequidt et al.[26]

In the following we present the results obtained with the different materials cited above.

4.1 nCB

In our previous work,[20] we chose the liquid crystal 5CB and measured γ_1 and γ_S by using method 1. To check if method 2 gave similar values for the bulk viscosity γ_1, we performed a new experiment with a homeotropic sample. We observed that in this sample the transition temperature T_{NI} was larger by about 0.2°C than in the samples treated with the polymercaptan. This indicates that the polymercaptan slightly dissolves in 5CB, mainly during the filling of the samples. Nevertheless, we observed an excellent agreement between the two methods on condition to plot the viscosity as a function of the temperature shift to the transition temperature T_{NI} (Figure 4a). This shows that the main effect of the polymercaptan pollution, which was similar in the other cyanobiphenyls, is to slightly shift the transition temperature, without changing in a measurable way the bulk viscosity. In Figure 4a, we also reported previous measurements of γ_1 by Wu and Wu [27] using the Frederiks transition and another set of data obtained by Siedler et al.[28]

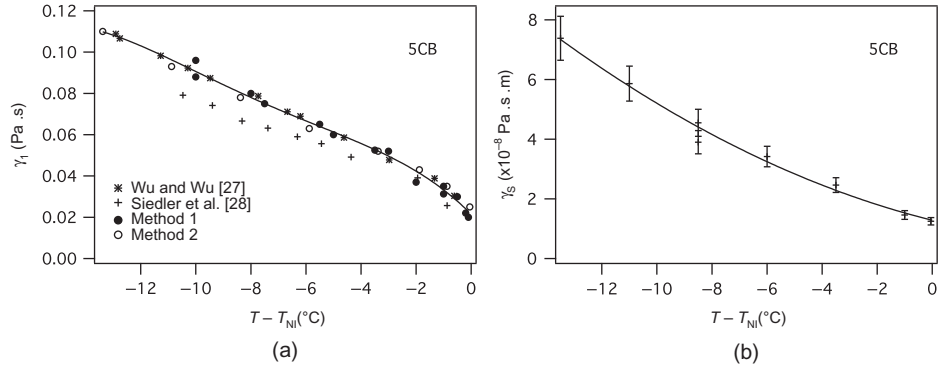

Figure 4. Bulk (a) and surface (b) viscosities of 5CB.

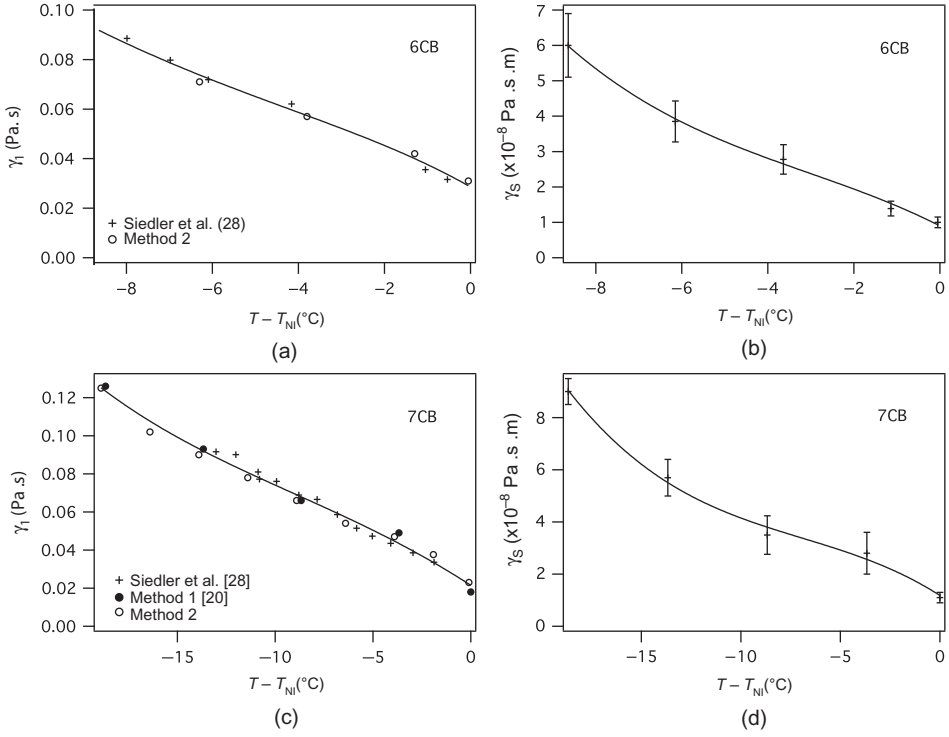

Figure 5. Bulk and surface viscosities of 6CB (a,b) and 7CB (c,d).

via direct torque measurements under rotating magnetic field. As can be seen, our results agree much better with those of Wu and Wu than with those of Siedler et al. This is comforting as the results of Wu and Wu have been recently checked by Caussarieu by using a very precise interferometric method to measure the Frederiks transition.[29] The values of the surface viscosity γ_S are shown in Figure 4b. We should note that the values given here are a bit smaller (by about 20%) than those given in our previous work.[20] This is due to the use of a new, slightly less viscous, sample of polymercaptan.

We then made similar measurements for the other members of the homologous series nCB. For 7CB and 8CB, we still used the two methods described above to determine γ_1, and we again observed a very good agreement between them. For this reason, we only used method 2 – easier to perform than method 1 – with the other members of the series. All our results for γ_1 and γ_S are shown in Figures 5 and 6. We emphasise that our results for γ_1 agree well with those of Siedler et al. except for 5CB.

4.2 MBBA

We observed that in the MBBA samples treated with the polymercaptan, T_{NI} immediately decreased by about 0.5°C after the sample was filled but then continued to rapidly decrease by about 5°C on the following day. This drift of T_{NI} is much faster than in cyanobiphenyls where 2 months were necessary to observe a similar effect. This observation shows that the polymercaptan dissolves much faster in MBBA than in cyanobiphenyls. In order to limit the effect of this pollution, we measured the viscosities in freshly prepared samples. The transition temperature was measured before and after each viscosity measurement and the samples in which T_{NI} had decreased by more than 1°C were systematically eliminated. These precautions being taken, we checked that the two methods described above gave similar values of γ_1 for similar temperature shifts $T - T_{NI}$. Our results for γ_1 are shown in Figure 7a and agree to within ±15% with those of Siedler et al.[28] and Kneppe et al.[30] obtained with pure materials. Our results for γ_S are shown in Figure 7b. Note that each point in this graph was obtained with a different sample.

4.3 Compensated mixture

In a previous work,[15] we measured the surface viscosity of a cholesteric liquid crystal composed of 50% by weight of 8OCB and 50% of CC. This mixture is compensated (i.e. has a nematic-like structure) at $T_c \approx 59$°C and melts at 67°C. In the vicinity of T_c, the equilibrium twist q changes rapidly with temperature

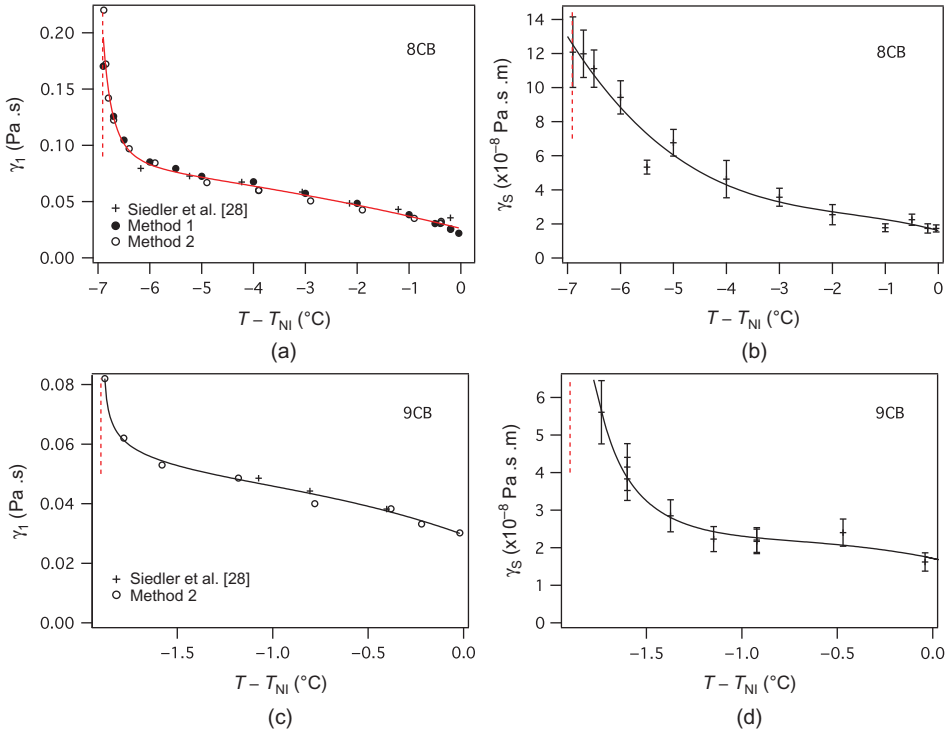

Figure 6. (colour online) Bulk and surface viscosities of 8CB (a,b) and 9CB (c,d). In each graph, the vertical dashed line indicates the nematic to smectic A transition temperature.

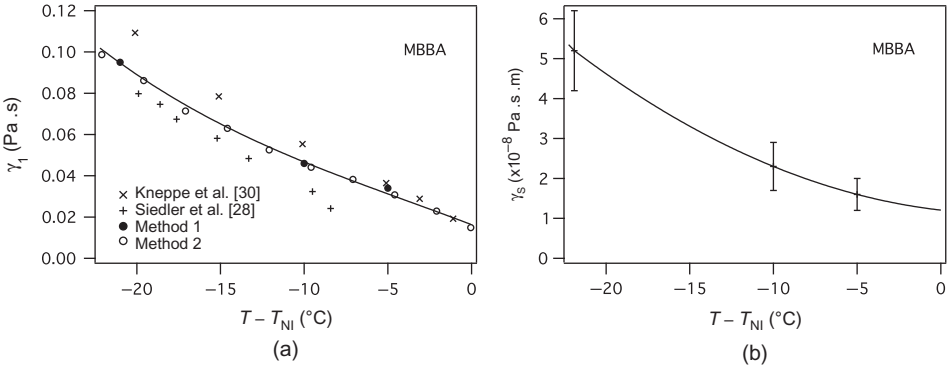

Figure 7. Bulk (a) and surface (b) viscosities of MBBA.

with a rate of change $dq/dT \approx 0.136\,\mu m^{-1}K^{-1}$.[26] This property was used to measure the surface viscosity at T_c at the interface with the polymercaptan. The technique consisted of submitting to temperature ramps samples treated with the polymercaptan on one side and for strong unidirectional planar anchoring on the other, and measuring simultaneously their optical transmittance between crossed polarisers. This method led to $\gamma_S = 3 \pm 1 \times 10^{-7}$ Pa s m at T_c. This value is of the same order of magnitude but larger than all the surface viscosities reported above. For this reason, we found it interesting to measure again the surface viscosity of this mixture with the rotating magnetic field technique. Our measurements were made at T_c with method 2 described above. Temperature T_c was determined by first aligning the magnetic field (at $B = 0.2$ T) with the polariser P_2 (see Figure B2) and then adjusting the temperature until optical extinction was observed between crossed polariser and analyser. Measurements with a homeotropic sample led to $\gamma_1 = 0.072 \pm 0.004$ Pa s by taking $\chi_a = 4 \pm 0.2 \times 10^{-7}$ (see Appendix 1). This value is in very good agreement with the value obtained by using the Frederiks transition: $\gamma_1 = 0.075 \pm 0.009$ Pa s.[15] As for the surface viscosity, we found $\gamma_S = 1.3 \pm 0.2 \times 10^{-7}$ Pa s m by taking $K_2 = 2.8 \pm 0.2$ pN.[26] This value is typically twice as

small as the one obtained with the ramp technique. An explanation could come from the lack of accuracy of the ramp technique that was particularly difficult to implement because of very delicate in situ temperature measurements. Another explanation could be that we used different samples of polymercaptan in the two experiments. It is clear that systematic measurements with samples of controlled viscosity should be performed to definitely resolve this issue.

5. Discussion

In the previous section, we displayed our viscosity measurements in separate graphs. A rapid examination shows that all viscosities have a common feature: they increase when the temperature decreases, more or less in the same proportion, with a stronger increase of both of them upon approaching the smectic A phase in the case of 8CB and 9CB (see Figure 6). For these two materials, a clear divergence of γ_1 is observed that was explained theoretically by Jähnig and Brochard [31] (according to these authors $\gamma_1 \propto \sqrt{\bar{\xi}}$, where $\bar{\xi}$ is the smectic correlation length that diverges at the transition). By contrast, γ_S does not seem to diverge, at least in 8CB, but we must be very cautious here because the values of K_2 which we used to calculate γ_S were perhaps underestimated close to the smectic phase. This could be the case if, in our samples, the nematic range was slightly larger than in the samples used by Madhusudana and Padmini.[23] Unfortunately, we cannot verify this point because these authors do not give the values of the transition temperatures of their samples.

The next question to address is to determine whether these two viscosities are correlated or completely independent. To answer this question, we plotted together in two graphs our viscosity measurements for all the nematic compounds studied. For more clarity, only the fits of the experimental data shown in the previous figures were reported (Figure 8). A rapid examination shows that all the curves are in the same order in the two graphs. This observation – which is the main result of the paper – clearly shows that γ_S and γ_1 are strongly correlated. In order to address this point further, we plotted in Figure 9 the length $l_S = \gamma_S/\gamma_1$ as a function of temperature. We find that in all compounds, l_S ranges in micrometer. More precisely, l_S ranges between 0.5 and 1 μm in the cyanobiphenyls and MBBA and is a bit larger $\sim 1.8\,\mu$m in the compensated mixture at T_c.

This now raises the question of how to interpret these results. The very large value of l_S with respect to molecular dimensions suggests that the surface dissipation is not localised to the surface but delocalised within a boundary layer of micrometric

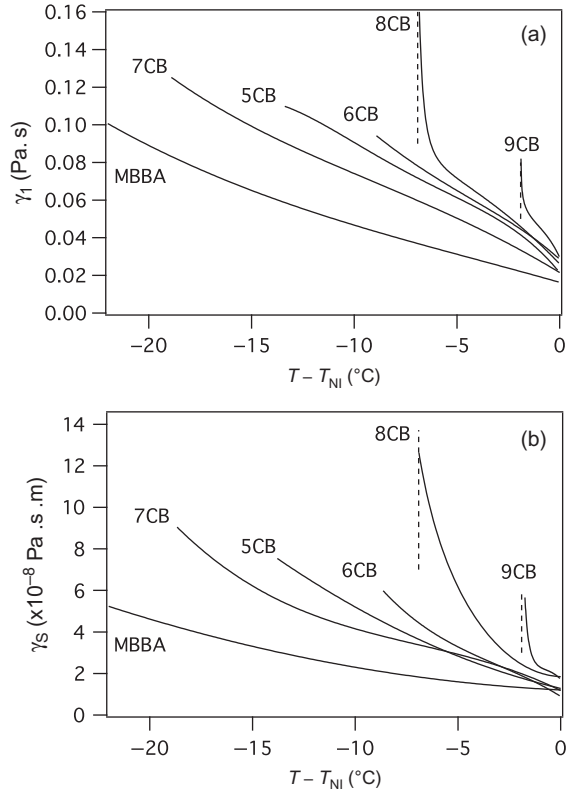

Figure 8. Overall presentation of bulk (a) and surface (b) viscosity measurements in the nematic samples.

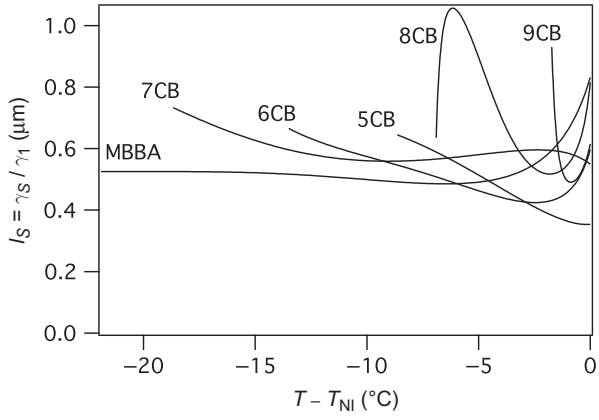

Figure 9. Ratio of the surface viscosity over the bulk viscosity as a function of temperature.

size. Note that similar models were already proposed by theorists.[5–7] The fact that there is an extra dissipation in this layer shows that the viscosity γ_1 increases inside before it drops abruptly at the polymer–nematic interface (where the nematic quadrupolar order parameter vanishes). In this scheme, we can imagine that the bulk viscosity increases exponentially from γ_1 to $\gamma_1 + \delta\gamma_1$ over the typical distance λ (as Barbero et al. did in Ref.[7]) and then vanishes over

a microscopic distance λ' much smaller than λ, characterising the thickness of the interface between the polymer and the nematic. In this case, the bulk torque Equation (3) remains unchanged, except that now γ_1 depends on z following the equation

$$\gamma_1(z) = \gamma_1 + \delta\gamma_1 \frac{\cosh\left(\dfrac{d-2z}{2\lambda}\right)}{\cosh\left(\dfrac{d}{2\lambda}\right)}. \tag{9}$$

Note that, for simplicity, we suppose that K_2 is constant in the whole sample thickness. To the bulk torque Equation (3), boundary conditions must be added:

$$\frac{\partial\alpha}{\partial z} = 0 \quad \text{at} \quad z = 0, d. \tag{10}$$

These conditions are equivalent to neglect the dissipation inside the polymer–nematic interface of microscopic thickness δ'.

Solving Equations (3), (9) and (10) in the limit $\omega \to 0$ yields $\phi(t) = \omega t - \alpha_e + \delta(z)$ with

$$\delta(z) = \frac{L^2\delta\gamma_1\lambda\omega}{K_2(L^2-\lambda^2)}\left[L\frac{\cosh\left(\dfrac{d-2z}{2L}\right)\tanh\left(\dfrac{d}{2\lambda}\right)}{\sinh\left(\dfrac{d}{2L}\right)} - \lambda\frac{\cosh\left(\dfrac{d-2z}{2\lambda}\right)}{\cosh\left(\dfrac{d}{2\lambda}\right)}\right]. \tag{11}$$

From this equation, we can calculate the retardation angle at the surfaces:

$$\alpha_S = \alpha_e + \frac{L^2\delta\gamma_1\lambda\omega}{K_2(L^2-\lambda^2)}\left[L\frac{\tanh\left(\dfrac{d}{2\lambda}\right)}{\tanh\left(\dfrac{d}{2L}\right)} - \lambda\right]. \tag{12}$$

In practice, $d \gg L$ and λ and $L \simeq \xi$ at small angular velocities, so that we can write

$$\alpha_S \simeq \alpha_e + \frac{\xi^2\delta\gamma_1\lambda\omega}{K_2(\xi+\lambda)}. \tag{13}$$

Finally, this expression reduces to Equation (7) with $\gamma_S = \delta\gamma_1\lambda$, when $\lambda \ll \xi$. In this limit, the two models are equivalent.

In our experiments, the model with the surface viscosity γ_S applies. This was shown explicitly in our previous paper.[20] As a consequence, the condition $\lambda \ll \xi$ must be fulfilled experimentally. In practice, $\xi > 2\,\mu\text{m}$, which indicates that λ should be much smaller than $2\,\mu\text{m}$. With the values of γ_S found before, this is the case if $\delta\gamma_1$ is of the order of $2-3\gamma_1$ or larger. In addition, we found that γ_S was roughly proportional to γ_1. This suggests that $\delta\gamma_1$ is also proportional to γ_1 on condition to suppose that λ is constant. All these conclusions are plausible in view of previous measurements of γ_1 in 5CB doped with polymetacrylate chains.[32] In these mixtures, it was experimentally found that $\delta\gamma_1/\gamma_1$ depends little on temperature and can be as large as 4 for a concentration of polymer of the order of 3% by weight.

6. Conclusion

To conclude, we have shown that the concept of surface viscosity was pertinent to explain the extra dissipation observed in samples treated for sliding planar anchoring with a polymercaptan layer. We have found that the surface viscosity scales like the bulk viscosity and that the length γ_S/γ_1 is in the micrometric range. This large value suggests a delocalised model for the viscosity, i.e. the existence of a nematic sublayer of a few tenths of a micrometer thick, in which the viscosity γ_1 increases significantly by a factor of 3–5 typically. A point that was not completely clarified concerns the divergence (or not) of the surface viscosity upon approaching the smectic A phase. This would require to know precisely the value of K_2 in the close vicinity of the nematic–smectic A transition, typically between T_{NA} and $T_{\text{NA}} + 0.2°\text{C}$, which was not the case in our experiments. Another interesting question to address would be to determine to what extent the surface viscosity depends on the shear viscosity of the polymer. This could be done by aging under UV exposure polymercaptan samples in order to increase their degree of polymerisation and viscosity. New experiments are planned in the near future to address these questions.

Acknowlegements

The authors are grateful to A. Pretrosyan for lending them his rubbing machine to prepare the planar samples and to A. Dequidt for fruitful comments. One of the authors (V.P.-N.) thanks Ecole Normale Supérieure de Lyon for scientific hospitality and acknowledges support from CNRS.

References

[1] Oswald P, Pieranski P. Nematic and cholesteric liquid crystals: concepts and physical properties illustrated by experiments. Boca Raton (FL): Taylor & Francis, CRC Press; 2005.

[2] Barbero G, Evangelista LR. Adsorption phenomena and anchoring energy in nematic liquid crystals. Boca Raton (FL): Taylor & Francis, CRC Press; 2006.
[3] Jerome B. Surface effects and anchoring in liquid-crystals. Rep Prog Phys. 1991;54:391–451.
[4] de Gennes PG. The physics of liquid crystals. Oxford: Clarendon; 1974. p. 97.
[5] Durand GE, Virga EG. Hydrodynamic model for surface nematic viscosity. Phys Rev E. 1999;59:4137–4142.
[6] Sonnet AM, Virga EG, Durand GE. Dilution of nematic surface potentials: relaxation dynamics. Phys Rev E. 2000;62:3694–3701.
[7] Barbero G, Dahl I, Komitov L. Continuum description of the interfacial layer of nematic liquid crystals in contact with solid surfaces. J Chem Phys. 2009;130:174902.
[8] Barbero G, Pandolfi L. Surface viscosity in nematic liquid crystals. Phys Rev E. 2009;79: 051701.
[9] Barbero G, Lenzi EK. Importance of the surface viscosity on the relaxation of an imposed deformation in a nematic liquid crystal cell. Phys Lett A. 2010;374:1565–1569.
[10] Teixeira de Souza R, Lenzi EK, Evangelista LR. Perturbative approach to the relaxation of the nematic deformation: surface viscosity and electric field. Mol Cryst Liq Cryst. 2011;546:57–66.
[11] Santoro PA, Silva AT, Lenzi EK, Evangelista LR. Surface viscosity and anchoring energy effects on the relaxation of a nematic liquid crystal cell. Liq Cryst 2012;39:647–654.
[12] Petrov AG, Ionescu ATh, Versace C, Scaramuzza N. Investigation of flexoelectric properties of a palladium-containing nematic liquid crystal, Azpac, and its mixture with MBBA. Liq Cryst. 1995;19:169–178.
[13] Mertelj A, Čopič M. Dynamic light scattering as a probe of orientational dynamics in confined liquid crystals. Phys Rev E. 2000;61:1622–1628.
[14] Vilfan M, Drevenšek Olenik I, Mertelj A, Čopič M. Aging of surface anchoring and surface viscosity of a nematic liquid crystal on photoaligning poly-(vinylcinnamate). Phys Rev E. 2001;63: 061709.
[15] Oswald P, Dequidt A, Żywociński A. Sliding planar anchoring and viscous surface torque in a cholesteric liquid crystal. Phys Rev E. 2008;77: 061703.
[16] Oswald P, Dequidt A. Direct measurement of the thermomechanical Lehmann coefficient in a compensated cholesteric liquid crystal. Europhys Lett. 2008;83:16005.
[17] Oswald P, Dequidt A. Measurement of the continuous Lehmann rotation of cholesteric droplets subjected to a temperature gradient. Phys Rev Lett. 2008;100:217802.
[18] Oswald P. About the Leslie explanation of the Lehmann effect in cholesteric liquid crystals. Europhys Lett. 2012;97:36006.
[19] Oswald P. Microscopic vs. macroscopic origin of the Lehmann effect in cholesteric liquid crystals. Eur Phys J E. 2012;35:10.
[20] Oswald P. Measurement with a rotating magnetic field of the surface viscosity of a nematic liquid crystal. Europhys Lett. 2012;100:26001.
[21] Brochard F, Léger L, Meyer RB. Freedericksz transition of a homeotropic nematic liquid crystal in rotating magnetic fields. J Phys (Paris). 1975;36:C1-209–C1–213.
[22] Bradshaw MJ, Raynes EP, Bunning JD, Faber TE. The Frank constants of some nematic liquid crystals. J Phys (Paris). 1985;46:1513–1520.
[23] Madhusudana NV, Pratibha R. Elasticity and orientational order in some cyanobiphenyls: Part IV. Reanalysis of the data. Mol Cryst Liq Cryst. 1982; 89:249–257.
[24] Leenhouts F, de Jeu WH, Dekker AJ. Physical properties of nematic Schiff's bases. J Phys (Paris). 1979; 40:989–995.
[25] Leenhouts F, Dekker AJ. Elastic constants of nematic liquid crystalline Schiff's bases. J Chem Phys. 1981;74:1956–1965.
[26] Dequidt A, Żywociński A, Oswald P. Lehmann effect in a compensated cholesteric liquid crystal: experimental evidence with fixed and gliding boundary conditions. Eur Phys J E. 2008;25:277–289.
[27] Wu ST, Wu CS. Experimental confirmation of the Osipov-Terentjev theory on the viscosity of nematic liquid crystals. Phys Rev A. 1990;42:2219–2227.
[28] Siedler LTS, Hyde AJ, Pethrick RA, Leslie FM. Zvetkow twist viscosity measurements of some nematic liquid crystals. Mol Cryst Liq Cryst. 1983;90:255–270.
[29] Caussarieu A. Fluctuations dans un système critique au voisinage d'une transition du second ordre [PhD thesis]. Lyon: Ecole Normale Supérieure de Lyon; 2013.
[30] Kneppe H, Schneider F, Sharma NK. Rotation viscosity 1 of nematic liquid crystals. J Chem Phys. 1982;77:3203–3208.
[31] Jähnig F, Brochard F. Critical elastic-constants and viscosities above a nematic-smectic. A transition of second-order. J Phys (Paris). 1974;35:301–313.
[32] Pashkovsky EE, Litvina TG. Influence of polymer molecules on the rotational viscosity and backflow effects at the bend Freederiks transition in nematic liquid crystals. Macromolecules 1995;28:1818–1824.
[33] Thoen J, Menu G. Temperature dependence of the static relative permittivity of Octylcyanobiphenyl (8CB). Mol Cryst Liq Cryst. 1983;97:163–176.

Appendix 1. Magnetic anisotropy of 8CB and the compensated mixture

It turns out that the magnetic anisotropy χ_a was not measured before in 8CB close to the smectic phase nor in the compensated mixture. To obtain χ_a, we measured the onset of instability of the Frederiks transition in 30 μm-thick planar samples. They were prepared between two Indium Tin Oxide (ITO) electrodes recovered with a thin 0825 polyimide layer (from Nissan Ltd.) rubbed in a single direction. Measurements of the critical voltages $V_c(B)$ at zero and 1 T magnetic field (with the field parallel to the anchoring direction) allowed us to obtain the ratio χ_a/ε_a of the magnetic over the dielectric anisotropy by using the formula

$$\frac{\chi_a}{\varepsilon_a} = \frac{\varepsilon_0\,\mu_0}{B^2}\,\frac{V_c^2(0) - V_c^2(B)}{d^2}. \qquad (A1)$$

The dielectric anisotropy was measured from capacity measurements in planar and homeotropic samples. Our data (which we do not give here) agree very well

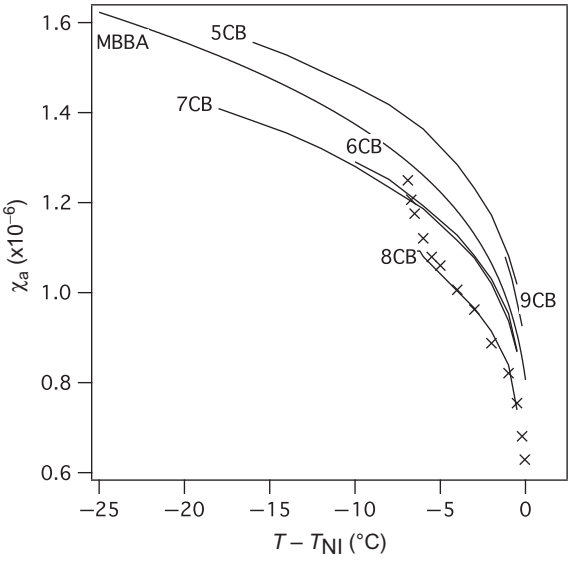

Figure A1. Magnetic anisotropy (in SI units) of 8CB and the other materials used in this work. The crosses are our experimental results. The solid line are taken from Ref.[22] for the cyanobiphenyls and from Ref.[24] for MBBA.

with those of Ref [33] for 8CB. As for the compensated mixture, we took the value $\varepsilon_a = 4.8$ given in Ref.[27]. Our results for 8CB are shown in Figure A1. They agree well with those given by Bradshaw et al.[22] far from the transition. For convenience, we also reported in this graph the values of χ_a for the other materials used in this work. As for the compensated mixture, we found $\chi_a = 4 \times 10^{-7}$ at the compensation temperature.

Appendix 2. Elastic constants of 9CB

We did not find in the literature the values of the elastic constants for 9CB. For this reason we measured ourselves these constants. First, we measured the dielectric anisotropy ε_a of the nematic phase. Our measurements were performed by capacitive measurements at 1 kHz in planar and homeotropic samples. Our results are shown in Figure B1. We then measured the splay elastic constant K_1 by measuring the critical voltage $V_c(1)$ of destabilisation of a planar sample and using formula $K_1 = \varepsilon_0 \varepsilon_a V_c(1)^2/\pi^2$. We took care of using a sample in which the two electrodes were rubbed in the same direction in order to limit the effect of the pretilt angle on the surfaces (of the order of 2° with the 0825 polyimide from Nissan used here). The precaution is essential to measure a correct value of K_1. Our results are shown in Figure B2. In order to measure the bend constant K_3 we used a special technique which was well suited to our experimental setup. More precisely, we measured the width of the 'splay-bend' Ising wall that spontaneously forms in homeotropic samples when they are placed at some distance of the

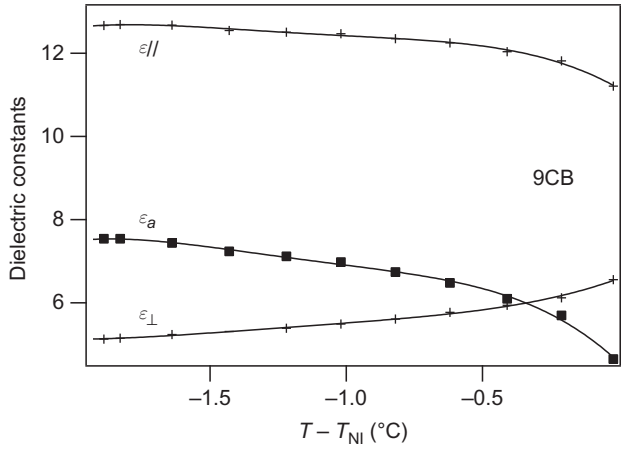

Figure B1. Dielectric constants and their anisotropy in 9CB. Solid lines are just a guide for the eye.

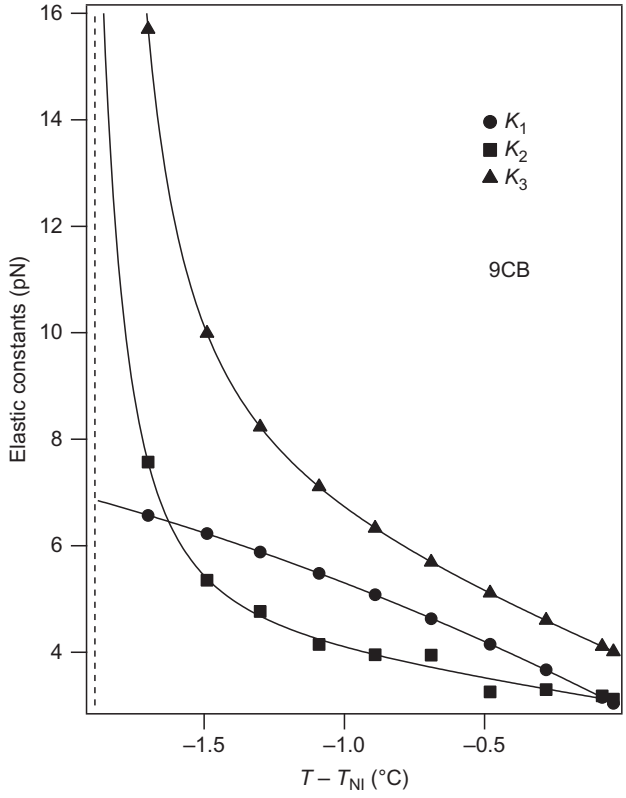

Figure B2. Elastic constants in 9CB. Solid lines are just a guide for the eye.

magnet. This wall forms because of the slight curvature of the magnetic field lines out of the magnet (Figure B3). It can be shown that the width of this wall depends on the local magnetic field and diverges when the magnetic field is smaller that the critical field $B_c = (\pi/d)\sqrt{\mu_0 K_3/\chi_a}$.[1] We measured experimentally the width of the wall as a function of the magnetic field by moving the sample along the revolution axis of the

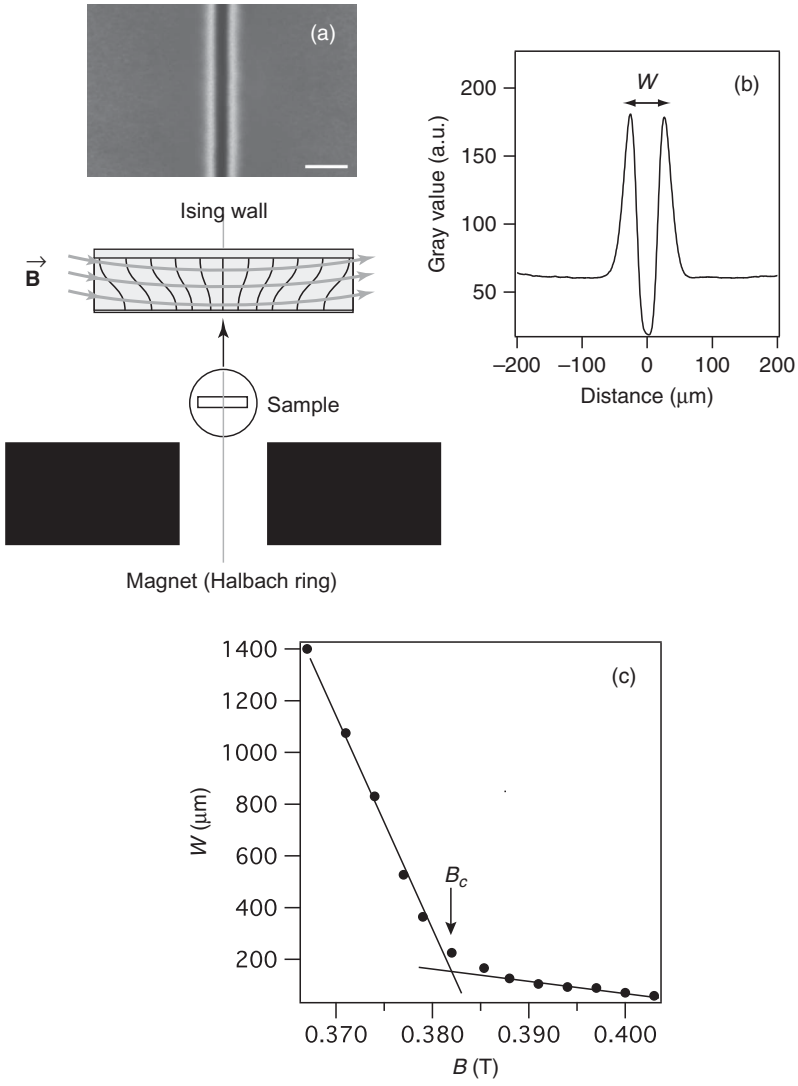

Figure B3. (a) Ising wall in a homeotropic sample of thickness $d = 30.3\,\mu$m. The image was taken at $B = 0.394\,T$ and temperature $T - T_{NI} = -1.61°$C between crossed polariser and analyser tilted by 45° with respect to the magnetic field. The white bar is 100 μm long; (b) Average intensity profile in the direction perpendicular to the wall and definition of the width W of the wall; (c) Width W as a function of the magnetic field. In this example $B_c = 0.382\,T$.

magnet. In this way, B_c was determined to within ±2%. To test this method, we first measured K_3 in 8CB and found values that agree with those of Madhusudana and Prahtiba [23] to within ±5%. We then measured K_3 in 9CB. Our results are shown in Figure B2. Finally, we determined K_2 indirectly by measuring the critical voltage $V_c(2)$ for the destabilization of a planar cell twisted by 90°. In this case, it can be shown that $K_2 = K_3/2 + 2K_1 - 2\varepsilon_0\varepsilon_a V_c(2)^2/\pi^2$.[1] This method is not very precise because the errors on K_1, K_3 and the term in $V_c(2)^2$ accumulate. For this reason, we estimate that our error on K_2 is not better than ±30%.